FULL PAPER

Extraordinary Macroscale Wear Resistance of One Atom Thick Graphene Layer

*Diana Berman, Sanket A. Deshmukh, Subramanian K. R. S. Sankaranarayanan, Ali Erdemir, and Anirudha V. Sumant**

During the last few years, graphene's unusual friction and wear properties have been demonstrated at nano to micro scales but its industrial tribological potential has not been fully realized. The macroscopic wear resistance of one atom thick graphene coating is reported by subjecting it to pin-on-disc type wear testing against most commonly used steel against steel tribo-pair. It is shown that when tested in hydrogen, a single layer of graphene on steel can last for 6400 sliding cycles, while few-layer graphene (3–4 layers) lasts for 47 000 cycles. Furthermore, these graphene layers are shown to completely cease wear despite the severe sliding conditions including high contact pressures (≈0.5 GPa) observed typically in macroscale wear tests. The computational simulations show that the extraordinary wear performance originates from hydrogen passivation of the dangling bonds in a ruptured graphene, leading to significant stability and longer lifetime of the graphene protection layer. Also, the electronic properties of these graphene sheets are theoretically evaluated and the improved wear resistance is demonstrated to preserve the electronic properties of graphene and to have significant potential for flexible electronics. The findings demonstrate that tuning the atomistic scale chemical interactions holds the promise of realizing extraordinary tribological properties of monolayer graphene coatings.

1. Introduction

Solid lubricants, such as, graphite, hexagonal boron nitride, molybdenum disulfide, boric acid are traditionally used by industry to combat friction and wear in a variety of moving mechanical assemblies.[1–4] They can be applied as thin or thick solid coatings or burnished and sprayed onto surfaces to achieve lubricity.[5] In all of these practices, the durability or lifetime remains as an important issue when especially very long wear life is desired.[6] In short, the most important quandary with all of these conventional solid lubricants has been how long the solid lubricant coatings will last. Additionally, in some specialty applications such as protective coatings for magnetic disc drives, an extremely thin coating (down to nm or less) providing low friction and wear characteristics is an essential requirement.[7,8]

Given the recent advances in the synthesis of graphene,[9] several studies have been carried out demonstrating the unique nanomechanical and nanotribological properties of single and few layer graphene.[10–12] While a few studies including our own have recently demonstrated the potential of few-layer graphene (pure or in additive form) in significantly reducing wear and friction in mechanical systems,[13–16] there are no reports on studying tribological behavior of single layer graphene at macroscales. From a fundamental scientific perspective, the origin of such dramatic improvements in wear resistance still remains an open question. Moreover, such an incredible wear resistance of few-layer graphene has raised the question as to how many sliding passes it would take to wear off one monolayer of graphene.

Here, we report the results of our tribology tests on a one layer thick graphene confined between a steel ball and a steel disk. Our previous studies suggest an inherent operational limitation of few-layer graphene imposed by the test environment;[14] it was shown that to work in humid environment, graphene requires occasional replenishment in the sliding contacts. To overcome this limitation and to elucidate the role of test environment, we performed our tests for both single layer graphene and few-layer graphene exposed to two different gases: hydrogen and nitrogen.

2. Results and Discussion

2.1. Graphene Lifetime in Hydrogen Environment

We experimentally demonstrate a unique tribological property of a single graphene layer: the lifetime of a monolayer of

Dr. D. Berman, Dr. S. A. Deshmukh,
Dr. S. K. R. S. Sankaranarayanan, Dr. A. V. Sumant
Center for Nanoscale Materials
9700 S. Cass Ave, Argonne National Laboratory
Argonne, IL 60439
E-mail: sumant@anl.gov
Dr. A. Erdemir
Energy Systems Division
9700 S. Cass Ave, Argonne National Laboratory
Argonne, IL 60439

DOI: 10.1002/adfm.201401755

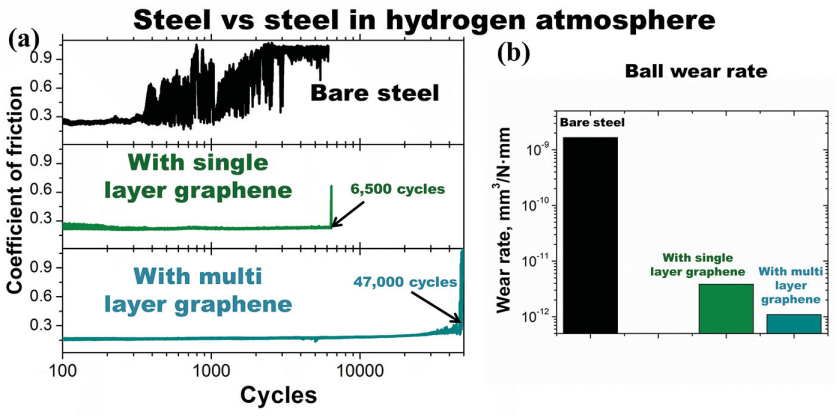

Figure 1. a) The coefficient of friction and b) wear rate for steel against steel sliding tribo-pairs in absence of graphene and in presence of single layer and few-layer graphene in hydrogen environment. The linear speed for all three tests in hydrogen environment was 9 cm/s.

graphene in hydrogen is shown to be more than 6400 cycles despite rather high contact pressure of 0.5 GPa between a steel ball and a steel disk. Most importantly, the 3D profile images demonstrate no evidence of any measurable wear on rubbing surfaces of steel disks. This finding suggests that the extraordinarily protective stability and wear resistance of graphene as a coating originates at the level of a single monolayer. As demonstrated in **Figure 1**, even one atom thick layer of graphene is shown to be sufficient to stop wear of rubbing disk surfaces and at the same time, keep friction constant and low (i.e., $\mu \approx 0.22$). As soon as the graphene layer wears out, friction increases steeply.

On Figure 1a, we show that the coefficient of friction for single layer graphene in-between two sliding steel interfaces is low and steady. The lifetime of this one layer graphene is nearly 6400 cycles when the test is performed in hydrogen environment (900 mbar) with exceptionally low wear rate of the steel ball side (Figure 1b) and with few-layer (3–4 layer thick flakes) graphene, the wear life can be further extended to 47 000 cycles with the wear rate of ball side reduced by almost 4 orders of magnitude (while no measurable wear could be recorded on the steel disk side). In the absence of graphene, a steel ball sliding against a steel disk in hydrogen environment results in the coefficient of friction increasing rapidly, within 300 cycles after starting the test and stabilizes to a high value of $\mu \approx 1$. This high friction leads to substantial amount of wear on rubbing surfaces of both the ball and the disk side as shown in Figure 1b.

In contrast, the wear mark on the ball side after such a long test in hydrogen environment in the presence of graphene is small and mostly identified by the Hertz contact diameter during sliding, which is ~60 µm for the test (for details See Supporting Information). The steel ball wear rate with graphene in Figure 1b overestimated due to not taking into account the ball's elastic deformation under such high contact pressure. Therefore, the actual reduction in the wear rate is even more substantial than 4 orders of magnitude.

Raman mapping (**Figure 2**) presents the evolution of the wear track coated with a single graphene layer during the sliding process in the hydrogen environment. The peak intensity of D (at ≈1360 cm^{-1}), G (at ≈1590 cm^{-1}), and 2D (at ≈2720 cm^{-1}) bands of graphene after an initial period of sliding (after 1000 cycles), in the middle of sliding (after 4000 cycles) and at the end of the tribological test (after 6500 cycles) are shown in Figure 2b, 2c, and 2d correspondingly. During continuous sliding, graphene gradually becomes damaged and highly disordered. This process results in a decrease in the 2D peak intensity, which is indicative of a loss of crystalline structure. Concurrently, the D-peak intensity increases, which indicates the defective or disorder nature of the graphene resulting perhaps from a mechanical rubbing action. Meanwhile, at the end of the test, when all the graphene is removed from the wear track, the 2D mapping indicates no carbon presence in the wear track, but only on its sides.

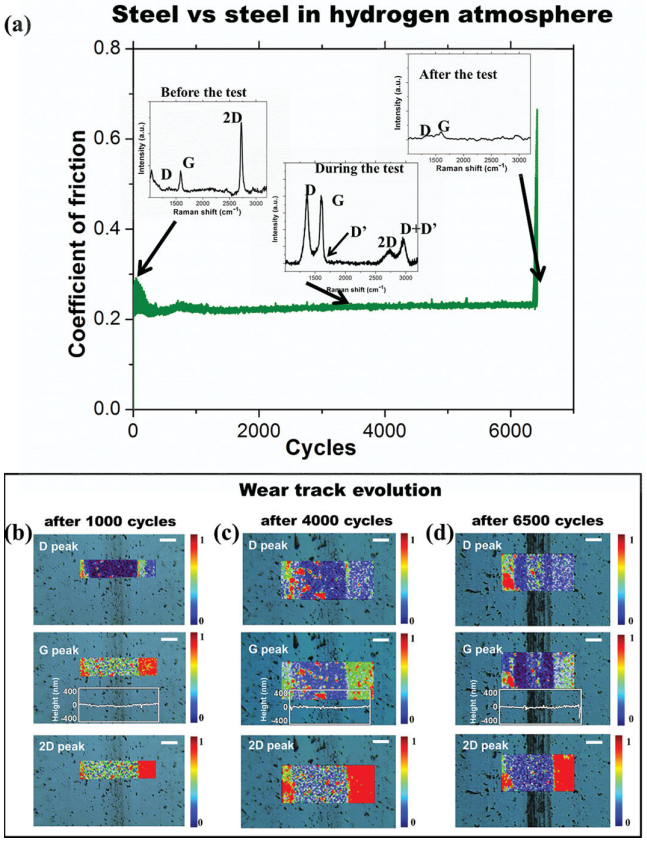

Figure 2. a) The coefficient of friction and the wear track evolution of the graphene-coated sample after b) 1000, c) 4000, and d) 6500 cycles is presented. Insets in (a) show typical Raman spectra from the wear track at the different time of the test. Cross-section line-profiles of the wear tracks are obtained using a 3D profilometer. The scale bar is 50 µm. Insets in (a) show the characteristic Raman signatures of the wear track before, during, and after the test. The linear speed for the test in hydrogen environment was 9 cm/s.

2.2. Graphene Lifetime in Nitrogen Environment

On the contrary, the single layer graphene does not survive for the long period of time in the case of dry nitrogen environment, which is provided as a reference to demonstrate the unique way by which hydrogen facilitates the extraordinary wear resistance of graphene. The coefficient of friction increases after several hundred cycles, indicating removal of graphene protection layer from the wear track (**Figure 3**). It should be mentioned that for a few-layer graphene this lifetime can be extended,[15,16] though it still remains considerably shorter than for graphene in hydrogen environment. Such a dramatic difference in the frictional behavior and lifetime of single layer graphene in the presence of hydrogen but not in nitrogen environment raises the question about the ambient gas effect on the atomic-scale friciton and wear mechanisms.

2.3. Environment Influence on Graphene

To better understand the origin of these differences, we performed reactive molecular dynamics simulations to model atomistic interactions during graphene's sliding behavior in different gaseous environments under severe contact pressure (**Figure 4**).

Sliding process under severe contact pressure of ≈0.5 GPa results in the partial rupture of graphene's honeycomb structure and leads to graphene flakes formation. When this fractured and defective graphene sheet is exposed to hydrogen, we see that hydrogen atoms occupy the reactive carbon edges of the flakes (Figure 4c,d). Hydrogen passivation stabilizes the defect sites on the flake, thus protecting the underlying surface from further damage. Hydrogen passivation of defect sites in other carbon systems such as diamond-like carbon (DLC) films[17] and in diamond films[18] and its effect in reducing adhesion and friction in self-mated contracts have been shown before, however, in this case, we observe that hydrogen passivation of graphene protects it from disintegration and helps in extending the wear life, which is unique and not observed before. The dynamical evolution of the passivation effect by hydrogen can be seen in Supporting Information. In case of dry nitrogen, almost no such passivation or repair of torn or broken graphene monolayers occurs and thus graphene experiences increasingly more fragmentation and loses its protective character upon cycling. Simulations suggest that nitrogen gas is mostly physisorbed[19] and does not react with carbon atoms at the edges of the flakes (Figure 4e,f). Failure to stabilize the defect sites results in rapid disintegration of defective graphene under high contact pressure and finally leads to formation of amorphous carbon (Figure S4 in Supporting Information). Indeed, Raman mapping (Figure 3c) of the wear track after the test in nitrogen indicates that carbon is still partially present at the wear track in the form of amorphous carbon which is not able to protect the sliding steel interfaces from high friction and wear.[20] Graphene disintegration in nitrogen results in the exposure of bare steel surface area to the sliding contact and leading to higher friction and wear. The above scenario also holds true under conditions of low load when graphene defects are randomly distributed (see Movies S1,S2 in Supporting Information).

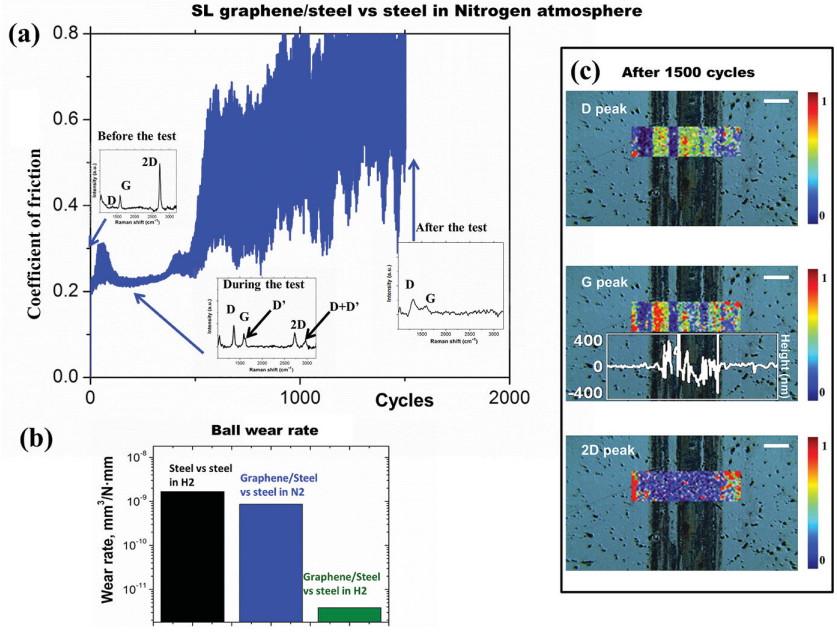

Figure 3. a) The coefficient of friction and b) wear rate for steel against steel sliding in presence of single layer graphene in dry nitrogen environment. Insets in (a) show typical Raman spectra from the wear track at the different time of the test. c) The chemical state of graphene in the wear track after 1500 wear cycles is presented by D,G, and 2D peak mapping. The cross-section line-profile of the wear track is obtained using 3D profilometer. The scale bar is 50 μm. The linear speed for the test in nitrogen environment was 7.8 cm/s.

We believe that the role of hydrogen is twofold: first, as a reactive gas it removes the excess of oxygen from the steel surfaces, thus suppressing iron oxides formation,[21,22] which is also supported experimentally by the fact that Raman spectrum of the wear track at the end of the test shows no iron oxide signature (≈1090 cm^{-1} and below).[14] Secondly, when and if graphene layer is damaged or ruptured, it instantly passivates the dangling carbon bonds and thus stabilizes the atomic array of graphene by forming covalent C-H bonds at the edges. The breaking and formation of bonds could be energetically favored due to the high contact pressures at the sliding interface. Indeed, it has been shown in previous DFT studies that the defect centers and edge sites represent stable chemisorption sites for hydrogen. While activation energies on pure graphene is ≈1.5 eV per hydrogen atom, it is much lower on defective sites (for example, 0.30 eV for SW defects, 0.93 eV for bivacancies).[23,24] In general, consistent with our predictions, it has been shown in several previous theoretical studies that saturating graphene edges with hydrogen lowers its energy and leads to a more stable structure.[25,26] We believe that our simulation results suggest one possible

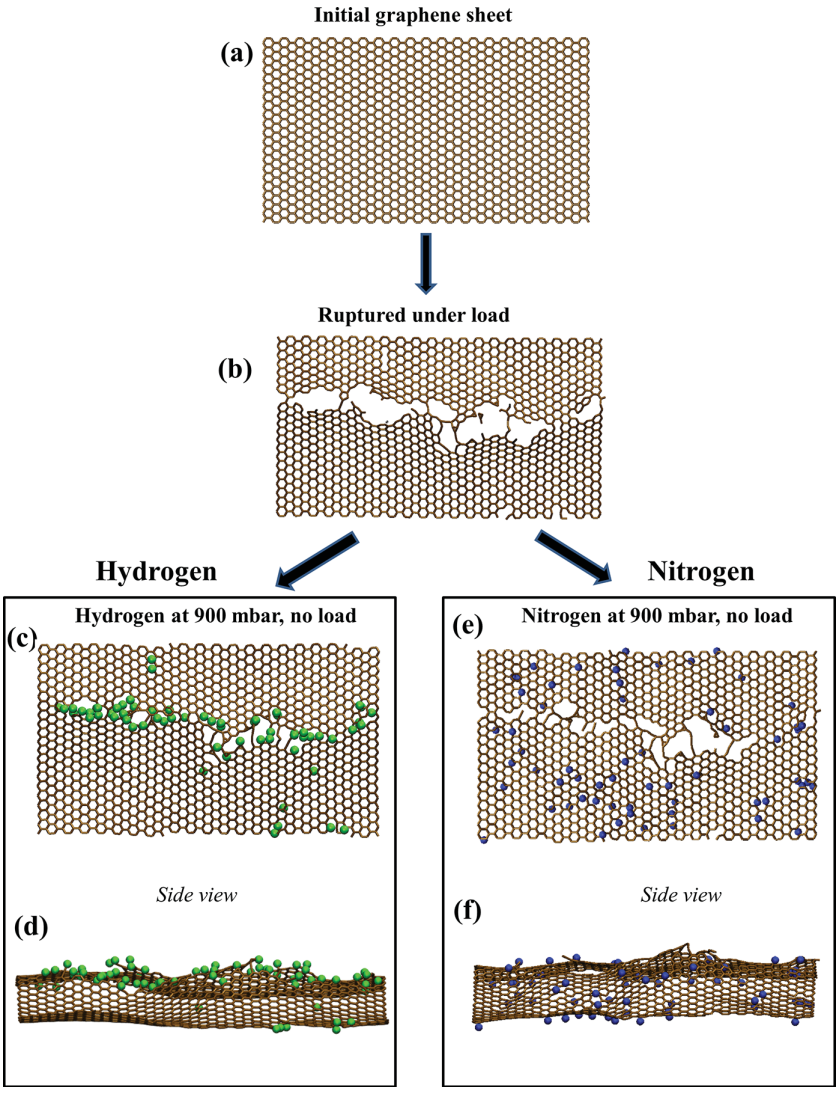

Figure 4. Graphene modifications under different atmospheres: a) Initial graphene sheet configuration, b) graphene ruptured under 0.5 GPa load in vacuum. c,d) Exposure to hydrogen atmosphere under no load results in hydrogen bonding to carbon atoms to stabilize the edges of graphene. e,f) In case of nitrogen atmosphere, no nitrogen bonding with the free carbon atoms at the edges of the flakes is observed and shown nitrogen is primarily physisorbed on the graphene surface. Green color corresponds to hydrogen atoms bonded to carbon and blue color corresponds to nitrogen atoms in close proximity to graphene sheet. Note, that only the atoms within 2 Angstrom distance from the surface of the graphene are shown for the sake of clarity.

scenario of hydrogen passivation helping to extend the lifetime of graphene within the wear track. Other scenarios can also exist. For example, an improved tribological performance of hydrogenated graphene was predicted by density functional theory (DFT) simulations[27] which attributed the observed frictional improvement to electronic contributions. Other possibilities also exist, including hydrogen induced formation of sp^3-like clusters[28,29] shown theoretically where interaction of hydrogen with few-layer graphene can induce formation of sp^3-like clusters through domino effect. Formation of extremely thin sp^3 rich layer could potentially increase the wear resistance. Although it is unlikely for this mechanism to manifest in a single graphene layer, it nonetheless remains an interesting possibility and cannot be ruled out in our case, which begs for more experimental and theoretical investigation in this direction.

An indirect evidence for chemically bonded hydrogen with graphene at the edges, is provided by the Raman analysis shown in Figure 2. The prominent D (at ≈1360 cm^{-1}) band and the appearance of the D' (≈1630 cm^{-1}) and D+D' (≈2960 cm^{-1}) bands are generally related to the point defects in the basal plane or edges of single-crystalline graphene domains,[20] which are observable for hydrogen terminated graphene.[30] Also, it was shown[31,32] that D' peak (≈1630 cm^{-1}) is much more pronounced in case of vacancy-type defects, resulting in lower $I_D/I_{D'}$ ratio in the order of ≈4, which increases up to ≈13 for the case of primarily sp^3 defects . Careful inspection of the Raman spectra for the wear track after 4000 cycles in hydrogen environment (Figure 2a) indicates the high intensity ratio of $I_D/I_{D'}$ (≈12), which corresponds to the defects primarily arising from sp^3 bonds, in our case C-H bonds formation. Raman analysis of the wear tracks after the COF increase in nitrogen environment indicates formation of amorphous carbon with $I_D/I_G \approx 2$ (in comparison to $I_D/I_G \approx 0.5$ for hydrogen environment), which corresponds to higher sp^2/sp^3 ratio in case of nitrogen than sp^2/sp^3 ratio for hydrogen run.[33]

2.4. Effect of Wear on the Electronic Properties of Graphene

To demonstrate the practical applicability of this extraordinary wear resistance of graphene and to further quantitatively evaluate the microstructural effects arising from the wear in the two different environments (hydrogen vs nitrogen) on the electrical conductivity, we perform non-equilibrium Green's function (NEGF) calculations using density functional theory (DFT). The NEGF-DFT technique used to evaluate the electronic transport employs a two-probe system; semi-infinite left- and right-electrode regions are in contact with a confined central scattering region. The NEGF-DFT calculations are carried out with the central scattering region representing the graphene sheets subjected to wear in the two different environment. In the case of pristine defect free graphene, as expected, we observe that the *I–V* characteristics are ohmic (**Figure 5**).

Figure 5 shows conductivities for the two graphene sheets which have undergone wear in hydrogen and nitrogen atmosphere. It can be clearly seen that the graphene sheets which have undergone little structural wear in the hydrogen

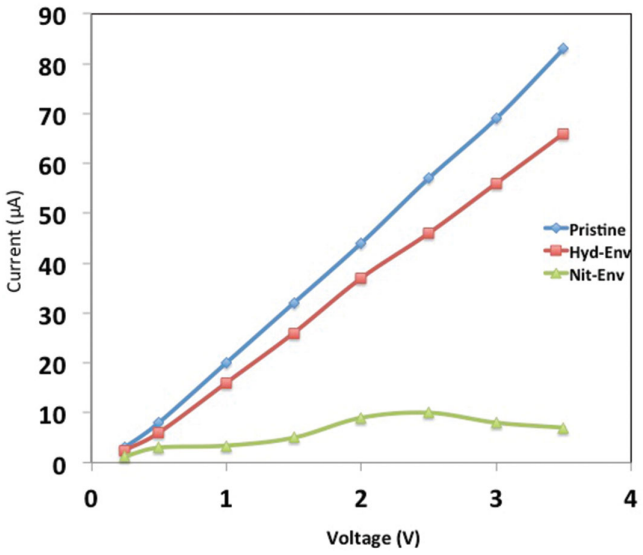

Figure 5. Theoretical estimates of graphene sheet conductivities after undergoing wear in two different environments (hydrogen vs nitrogen). First-principles based non-equilibrium Green's function calculations of the conductivity are used to evaluate the electronic properties and to demonstrate the practical applicability of the improved wear resistance in the area of flexible electronics.

environment still maintain their ohmic characteristics and show very little change in their electronic conducitivity. In contrast, the graphene sheets that were subjected to wear in a nitrogen environment are highly defective and therefore a significant deviation from ohmic behavior is observed. The reduced wear of graphene translates into improved electrical characteristics and demonstrates that the observed improvements in wear performance have an important role to play in the area of flexible electronics. This also demonstrates that the wear resistant graphene layers have a significant potential as stretchable and flexible electronic materials with possible applications ranging from flexible sensor tapes for monitoring structural integrity, active antennas, printer cables, and flexible components for communications (cell phones), neural probes, biotic-abiotic interfaces, and painless drug delivery systems.[3]

3. Conclusion

In summary, our findings indicate that the macroscale wear resistance of single layer graphene is truly extraordinary when compared to other commonly used solid lubricants. The wear rate of the commonly used steel protective thin film coatings, such as MoS_2,[34] and diamond like carbon (DLC),[35] usually varies as 10–1000 monolayers per 1000 cycles depending on the operating conditions. We have thus demonstrated another facet of one-atom thick graphene layer's extraordinary property, which suppresses both friction and wear of the underlying surface and stays for as long as 6400 cycles. Thus, apart from being one of the strongest materials known,[36,37] our study indicates that graphene is also the most wear resistant material ever known. We show by means of NEGF-DFT calculations that the improved wear resistance preserves the electronic properties of graphene and has significant potential in the area of flexible electronics.

4. Experimental Section

Deposition of Single and Few-Layer Graphene on Steel Substrate: The majority of the tribo tests were concentrated on using single layer graphene between two sliding steel interfaces. Single layer graphene film was grown on copper foil using the widely established chemical vapor deposition method.[38,39] Thickness of as-grown graphene was checked using Raman Spectroscopy. After deposition the graphene layer is removed from one side of copper foil using oxygen plasma reactive ion etching (RIE) procedure. To provide a mechanical support to graphene during transfer process a ≈300 nm thick poly(methyl methacrylate) (PMMA) protective layer is used. After that, the Cu foil was etched with ammonium persulfate (0.1 M, Sigma Aldrich) and the PMMA/graphene film was rinsed in distilled water and lowered on stainless steel (440 C grade) substrate with rms roughness R_q = 20 nm. The PMMA protective layer was removed using acetone to provide a single-later graphene on steel flat sample. Special care was taken to make sure that there is no left-over PMMA on the surface and it was confirmed by extensive Raman mapping of the surface (**Figure 6**). In case of few-layer graphene coating on the steel surface, graphene few-layer flakes were deposited on the steel substrate from graphene containing ethanol solution and then ethanol is evaporated in dry nitrogen flow. Solution-processed graphene was prepared by chemical exfoliation of highly oriented pyrolytic graphite (HOPG) and was then suspended in ethanol (Graphene Supermarket Inc.). The weight concentration of graphene was 1 mg/L containing mostly single layer graphene. Small SPG amount (10–15 drops or 0.5–0.75 mL of solution per 1 cm^2) was applied on the highly polished surfaces of stainless steel plates in a colloidal liquid state and the liquid ethanol part was evaporated in dry nitrogen environment to prevent graphene oxide formation. The procedure resulted in few-layer (3–4 layers) graphene flakes on the steel substrate.

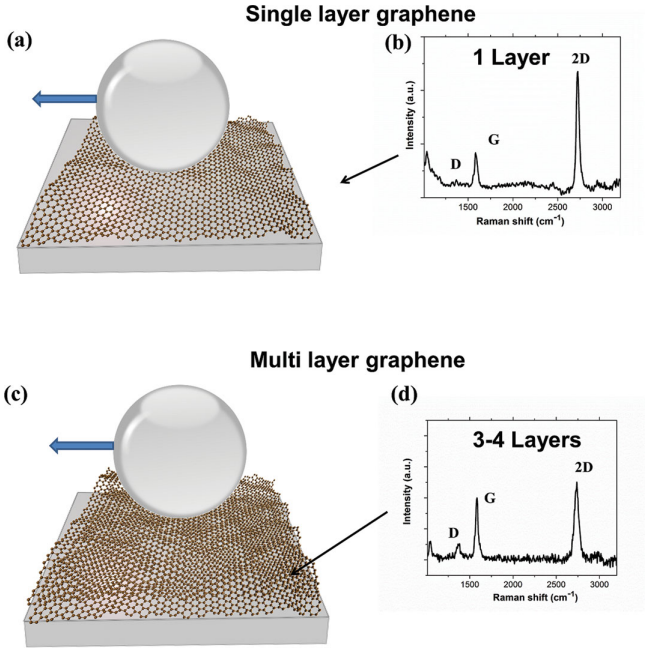

Figure 6. Schematic of the experimental setup and the Raman spectra of transferred single-layer graphene on steel (a and b) and few-layer graphene (c and d) correspondingly.

Tribological Tests Procedure: The counterpart in the tribological tests was a stainless steel ball (440 C grade) of 9.5 mm diameter with rms roughness R_q = 15 nm measured by the 3D profilometer. Macro-scale tribological tests were performed in dry hydrogen (900 mbar) and dry nitrogen (900 mbar) environments at room temperature using a CSM tribometer with a ball-on-disk contact geometry. The normal load during the tribotests was 1 N (Hertz maximum contact pressure 0.5 GPa) at a speed of 60 rpm, and the radius of the wear track varying from 5 mm up to 15 mm (the linear speed varied from 3 cm/s up to 9 cm/s). The assessment of the wear volume of flat was very difficult as wear was manifested as deep scratches and could not be fit into a reliable wear equation. To estimate the wear volume for the balls after the tribo tests, we used the following equation:

$$V = \left(\frac{\pi h}{6}\right)\left(\frac{3d^2}{4} + h^2\right) \quad (1)$$

where

$$h = r - \sqrt{r^2 - \frac{d^2}{4}} \quad (2)$$

d is wear scar diameter and r is the radius of the ball.

Optical Microscopy and Raman Spectroscopy: The imaging of the wear scars was performed with an Olympus UC30 microscope. The wear rates on the ball and the flat sides were determined with a 3D non-contact MicroXam profilometer. Characterization of deposited graphene layer and wear debris after the tribotests is performed by an Invia Confocal Raman Microscope using the blue laser light (λ = 442 nm). The accumulation time for each spectrum in the single scan mode and for the mapping is 10 s.

Molecular Dynamic Simulations: Reactive molecular dynamics (MD) simulations with dynamic charge transfer between atoms is used to investigate the effect of gas phase environment on the fracture and passivation mechanisms under GPa loads. To simulate the graphene interaction with hydrogen and nitrogen environment after a wear cycle, we utilize molecular dynamic (MD) simulations employing a reactive force-field (ReaxFF) potential model that allows for variable and dynamic charge transfer between atoms. In particular, reactive force-field (ReaxFF) implements the feature of quantum chemistry calculations, including molecular association/dissociation and charge transfer between cations and anions, and therefore ensure a more accurate description of the oxidation simulation. By calculating many-body interactions of a single particle, characteristics of quantum chemistry effect are employed in multiple-components of particle interactions as shown in Equation 3, such as bond energy, over/under coordination, lone-pair energy, valence angle, torsion, hydrogen bond, van der Waals, and Coulomb:[40]

$$E_{total} = E_{bond} + E_{over} + E_{under} + E_{lp} + E_{val} + E_{tors} + E_{H} + E_{vdw} + E_{Coul} \quad (3)$$

Additionally, the temporal charges of cations/anions are calculated using the electro-negativity equalization method as shown in Equation 4:

$$E(q) = \sum_i \left[\chi_i q_i + \eta_i q_i^2 + Tap(r_{ij}) k_c \frac{q_i q_j}{\left(r_{ij}^2 + \gamma_{ij}^{-3}\right)^{1/3}} \right] \quad (4)$$

In the above equation, q, χ, η, $Tap(r)$, γ, and k_c are ion charge, electro-negativity, atomic hardness, 7th order taper function, shielding parameter, and dielectric constant, respectively. Detailed implementation and development of ReaxFF models for C-H-N interactions can be found in the work by van Duin et al.[41] It is capable of treating both metallic and ceramic systems as well as bond formation and bond breakage involved in the graphene nucleation and growth processes. Additionally, it can take into account the presence of multiple coordination as well as valence states when the graphene film interacts with hydrogen and/or nitrogen. The simulation set-up and computational details are summarized in supporting information.

Calculation of Electric Conductivity using NEGF-DFT Simulations: The electronic transport of the graphene junctions (pristine as well as those undergoing wear in hydrogen and nitrogen environment) was investigated in order to reveal the conductivity mechanism and the I-V characteristics. The calculations were performed with the ATK package, in which the DFT is combined with non-equilibrium Green's function method to calculate the electronic and transport properties of nanoscale systems. The current $I(V)$ is determined by the transmission coefficient $T(E,V)$, which is a function of the energy E and bias voltage V, through the Landauer-Büttiker formula, $I(V) = (2e/h)\int T(E,V)[f_l(E) - f_r(E)]dE$ where $f_{l/r}$ is the Fermi distribution function of the left/right electrodes. In the calculation, the local density approximation in the form of the Perdew and Zunger exchange-correlation functional is used. Only valence electrons are self-consistently calculated in the calculation, and the atomic cores are described by standard norm conserving pseudo-potentials. The valence wave functions are expanded by localized numerical (pseudo) atom orbitals, with the single zeta plus polarization basis set for Au atoms and the double zeta plus polarization basis set for amorphous carbon. The k-point sampling is 2, 2, and 100 in the x, y, and z directions, where z direction is the transport direction, which was enough to give the converged results. Before calculating the electron transport properties, we first carried out MD simulations as described in the previous section to generate the various configurations.

Supporting Information

Supporting Information is available from the Wiley Online Library or from the author.

Acknowledgements

Use of the Center for Nanoscale Materials was supported by the U. S. Department of Energy, Office of Science, Office of Basic Energy Sciences, under Contract No. DE-AC02–06CH11357. This research used resources of the National Energy Research Scientific Computing Center, a DOE Office of Science User Facility supported by the Office of Science of the U.S. Department of Energy under Contract No. DE-AC02-05CH11231.

Received: May 30, 2014
Revised: July 10, 2014
Published online: August 26, 2014

[1] A. Erdemir, Solid Lubricants and Self-lubricating Films, in *Handbook of Modern Tribology*, (Ed. B. Bhushan) CRC Press **2001,** 787–818.
[2] S. Chu, A. Majumdar, *Nature* **2012**, *488*, 294–303.
[3] A. Erdemir, J. M. Martin, *Superlubricity*, Elsevier, Amsterdam **2007**.
[4] T. W. Scharf, S. V. Prasad, *J. Mater. Sci.* **2013**, *48*, 511–531.
[5] B. Bhushan, B. K. Gupta, *Handbook of tribology: materials, coatings, and surface treatments*, **1991**.
[6] J.-M. Martin, *Nanolubricants*(Tribology in practice series) **2008**.
[7] R. J. Yeo, E. Rismani, N. Dwivedi, D. J. Blackwood, H. R. Tan, Z. Zhang, S. Tripathy, C. S. Bhatia, *Diam. Relat Mater.* **2014,** *44,* 100–108.
[8] A. C. Ferrari, *Surf. Coat. Technol.* **2004**, *180–181*, 190–206.
[9] A. K. Geim, K. S. Novoselov, *Nat. Mater.* **2007**, *6*, 183–191.
[10] L. Xu, T. B. Ma, Y. Z. Hu, H. Wang, *Nanotechnology* **2011**, *22*, 285708.
[11] Z. Deng, A. Smolyanitsky, Q. Li, X. Q. Feng, R. Cannara, *Nat. Mater.* **2012**, *11*, 1032–1037.
[12] C. Lee, Q. Li, W. Kalb, X.-Z. Liu, H. Berger, R. W. Carpick, J. Hone, *Science* **2010**, *328*, 76–80.

[13] S. S. Kandanur, M. A. Rafiee, F. Yavari, M. Schrameyer, Z. Z. Yu, T. A. Blanchet, N. Koratkar, *Carbon* **2012**, *50*, 3178–3183.
[14] D. Berman, A. Erdemir, A. V. Sumant, *Carbon* **2013**, *54*, 454–459.
[15] D. Berman, A. Erdemir, A. V. Sumant, *Carbon* **2013**, *59*, 167–175.
[16] D. Berman, A. Erdemir, A. V. Sumant, *Mater. Today* **2014**, *17*, 31–42.
[17] J. D. Schall, G. Gao, J. A. Harrison, *J. Phys. Chem. C* **2010**, *114*, 5321–5330.
[18] A. V. Sumant, D. S. Grierson, J. E. Gerbi, J. A. Carlisle, O. Auciello, R. W. Carpick, *Phys. Rev. B* **2007**, *76*, 235429.
[19] A. V. Vernos, W. A. Steele. *Langmuir* **1986**, *2*, 606–612.
[20] A. C. Ferrari. *Solid State Commun.* **2007**, *143*, 47–57.
[21] W. K. Jozwiak, E. Kaczmarek, T. P. Maniecki, W. Ignaczak, W. Maniukiewicz, *Appl. Catal. A* **2007**, *326*, 17–27.
[22] O. Kubaschewski, C. Alcock, P. Spencer, *Materials Thermochemistry*, 6th ed., Pergamom Press, Oxford **1993**.
[23] D. W. Boukhvalov, M. I. Katsnelson, *Nano Lett.* **2008**, *8*, 4373–4379.
[24] D. W. Boukhvalov, M. I. Katsnelson, A. I. Lichtenstein, *Phys. Rev. B* **2008**, *77*, 035427.
[25] K. He, G.-D. Lee, A. W. Robertson, E. Yoon, J. H. Warner, *Nat. Commun.* **2014**, *5*, 3040.
[26] C. Bores, I. Cabria, J. A. Alonso, M. J. Lopez, *J. Nanopart. Res.* **2012**, *14*, 1263.
[27] J. Wang, F. Wang, J. Li, S. Wang, Y. Song, Q. Sun, Y. Jia, *Tribol. Lett.* **2012**, *48*, 255–261.
[28] S. Rajasekaran, F. Abild-Pedersen, H. Ogasawara, A. Nilsson, S. Kaya, *Phys. Rev. Lett* **2013**, *111*, 085503.
[29] A. G. Kvashnin, L. A. Chernozatonskii, B. I. Yakobson, P. B. Sorokin, *Nano Lett.* **2014**, *14*, 676–681.
[30] Z. Luo, T. Yu, K. Kim, Z. Ni, Y. You, S. Lim, Z. Shen, S. Wang, J. Lin, *ACS Nano* **2009**, *7*, 1781–1788.
[31] A. Eckmann, A. Felten, A. Mishchenko, L. Britnell, R. Krupke, K. S. Novoselov, C. Casiraghi, *Nano Lett.* **2012**, *12*, 3925–3930.
[32] A. Ferrari, J. Robertson, *Phil. Trans. R. Soc. Lond. A* **2004**, *362*, 2477–2512.
[33] F. C. Tai, S. C. Lee, C. H. Wei, S. L. Tyan, *Mater. Trans.* **2006**, *47*, 1847–1852.
[34] M. Chhowalla, G. Amaratunga, *Nature* **2000**, *407*, 164–7.
[35] A. Erdemir, C. Donnet, *J. Phys. D. Appl. Phys.* **2006**, *39*, R311–R327.
[36] C. Lee, X. D. Wei, J. W. Kysar, J. Hone, *Science* **2008**, *321*, 385.
[37] G. H. Lee, R. C. Cooper, S. J. An, S. Lee, A. van der Zande, N. Petrone, A. G. Hammerberg, C. Lee, B. Crawford, W. Oliver, J. W. Kysar, J. Hone, *Science* **2013**, *30*, 1073–1076.
[38] K. S. Kim, Y. Zhao, H. Jang, S. Y. Lee, M. K. Kim, K. S. Kim, J.-H. Ahn, P. Kim, J.-Y. Choi, B. Hee, *Nature* **2009**, *457*, 706–710.
[39] X. S. Li, W. W. Cai, L. Colombo, R. S. Ruoff, *Nano Lett.* **2009**, *9*, 4268–4272.
[40] C. F. Sanz-Navarro, P.-O. Aįstrand, D. Chen, M. Rønning, A. C. T. van Duin, T. Jacob, W. A. Goddard, *J. Phys. Chem. A* **2008**, *112*, 1392–1402.
[41] A. C. T. Van Duin, S. Dasgupta, F. Lorant, W. A. Goddard. *J. Phys. Chem. A* **2001**, *105*, 9396–9409.